Assessing internal erosion in a rigid wall-permeameter: theoretical and experimental aspects

A. M. Molina-Gomez, R. P. Chapuis
Department CGM, Ecole Polytechnique, Montreal, QC, Canada

ABSTRACT
The risk of internal erosion was assessed for a crushed stone, theoretically and experimentally. The theoretical risk was assessed with different methods, all based on the characteristics of the grain size distribution curve. The real risk was evaluated by tests in a clear-wall rigid-wall permeameter, equipped with five lateral piezometers. Precautions were taken to start with a homogenous specimen, and start with a fully saturated condition. At the beginning of each test, the local gradient values were equal, indicating a homogeneous specimen. Many physical results, collected during each test, are presented. The displacement of fine particles was observed and documented. The hydraulic conditions included a series of steps, each with a mean constant gradient. Each experiment included series of either upward or downward vertical seepage to assess the influence of the flow direction upon the internal erosion process. During the tests internal erosion created preferential seepage paths, which were visually identified using coloured water as a tracer. In addition, several non-reactive tracer tests were conducted at different gradient steps, which enabled to quantify a reduction in effective porosity during the internal erosion process, due to the creation of preferential seepage paths.

RÉSUMÉ
Le risque d'érosion interne a été évalué pour une pierre concassée, en théorie et en pratique. Le risque théorique a été évalué par différentes méthodes, toutes basées sur la courbe granulométrique. Le risque réel a été évalué par des essais en perméamètre à paroi rigide et transparente, équipé de cinq piézomètres latéraux. Des précautions ont été prises pour débuter avec un spécimen homogène et dans des conditions saturées à 100%. Au début de chaque test, les valeurs locales du gradient étaient égales, indiquant un spécimen homogène. De nombreux résultats physiques, recueillis pendant les essais, sont présentés. Le déplacement des fines particules a été observé et documenté. Les conditions hydrauliques incluaient une série d'étapes à gradient moyen constant. Chaque expérience incluait des séries d'étapes à écoulement vertical ascendant ou descendant pour évaluer l'influence de la direction sur l'érosion interne. Pendant les essais, l'érosion interne a créé des chemins préférentiels d'écoulement, visuellement identifiés par de l'eau colorée utilisée comme traceur. De plus, plusieurs essais de traceur non réactif ont été menés à différentes étapes de gradient, ce qui a permis de quantifier la réduction de la porosité effective pendant le processus d'érosion interne, à cause de la création de chemins préférentiels.

1 INTRODUCTION

Internal erosion is known to be responsible for many disorders (which include failures) in civil engineering projects. Foster et al. (2000) examined the disorder of over eleven thousand dams and found that internal erosion was involved in about 46% of instabilities. For highway pavements, there was no similar study. However, internal erosion is the probable cause of many disorders (e.g., Chapuis et al. 1996). These include poor drainage in the thaw period after winter, or capillary retention in structural layers, with dilation during freezing, resulting in winter road bumps and then potholes after thawing.

When a non-plastic material is considered for use in a project, the designer may verify its grain size distribution curve (GSDC) and use a few criteria to assess whether or not the fine particles of this soil can move in the soil pore space, which defines internal erosion. This phenomenon may be produced by seepage and vibration, either alone or combined. It yields heterogeneous soil layers. Early warnings of the risk of internal erosion are visible segregation during transport, placement, and compaction. More segregation is due to mechanical actions such as vibration, seepage, or freeze-thaw cycles. When segregation occurs in one layer, the filtering criteria between the two adjacent layers (above and below) may be no longer satisfied, which may cause severe damage to engineered facilities. This is why the problems of filtering and internal erosion are important.

This paper deals with internal erosion of a 0-5 mm crushed stone that may be used in various projects of civil and mining engineering. The paper briefly presents the available theories to predict the risk of internal erosion. These are applied to the material under study. Then, experimental results are presented for permeability tests performed in rigid-wall permeameters, with several steps of constant mean gradient. They include the variation of hydraulic conductivity during the internal erosion process. The displacement of fine particles was registered through the permeameter clear wall. A few preferential seepage paths developed during the process: they could be seen with coloured water as a tracer. In addition, several non-reactive tracer tests were carried out at different gradient steps, which gave the value of effective porosity for the specimen during the on-going erosion process, due to the creation of preferential seepage paths.

2 THEORIES TO PREDICT INTERNAL EROSION

Several methods are available to predict internal erosion. These use the GSDC and geometric criteria. Currently, engineering consultants use three sets of old criteria for internal erosion: the early ones of Lubochkov (1965, 1969) as improved by Kenney and Lau (1985, 1986), those of Kezdi (1969), and those of Sherard (1979). Many recent studies have investigated well-graded and gap-graded soils before proposing new internal stability criteria (Chang and Zhang, 2013a, b; Li and Fannin 2008, 2012; Wan and Fell 2008).

The risk assessment usually proceeds with the filter criteria for two adjacent soils. It works as follows: (i) split the soil GSDC at a selected grain size, which yields a fine fraction and a coarse fraction; (ii) verify the filter criteria for the resulting GSDCs of the two fractions as if they were two adjacent soils. This is a long process, even with a spreadsheet, because it involves successive splits and calculation of the two resulting GSDCs before applying the filter criteria.

To shorten this long process, Chapuis (1992) wrote the filter criteria inequalities as equations for the GSDC slope in the usual plot of y = % solid mass passing versus x = log (d / 1 mm). The filter criteria involve sizes d_{15}, d_{50} and d_{85} of the two GSDCs, where d_x is the size such as x% of the solid mass is smaller than d_x. The coarse and fine fractions are given indexes c and f. For example, d_{85c} is the size such as 85% of the solid mass of the coarse fraction is smaller than d_{85c}. From the mathematics, Chapuis (1992) derived geometric criteria that are easy to verify by graphical techniques. Chapuis and Tournier (2006) improved these to assess the internal erosion risk.

2.1 The old criteria for non-plastic soils

Kezdi (1969) developed a method where $d_{15c}/d_{85f} < 5$ and $d_{15c}/d_{15f} > 4$. The first inequality means that if a portion of the GSDC has a slope flatter than 24.9% per log cycle, the soil will be unable to retain its particles finer than the size at which such slope occurs (Chapuis 1992). The second inequality of Kezdi (1969) was not used for the graphical equivalence.

Sherard (1979) proposed a method with $d_{15c}/d_{85f} < 5$. Graphically, it means that if a portion of the GSDC has a slope flatter than 21.5% per log cycle, the soil will be unable to retain its particles finer than the size at which such slope occurs (Chapuis 1992).

Kenney and Lau (1985, 1986) developed a more complex method, which refers to the work by Lubochkov (1965; 1969). Graphically, their method works as follows. Select a GSDC point of abscissa d_x and ordinate y_x = percentage passing. At this point, the slope of the GSDC must be higher than that of the curve of Eq, 1 to have internal stability (Chapuis 1992):

$$y / y_x = (d / d_x)^{0.7213} \quad (1)$$

For the small particles, Eq. 1 gives: at d_5, the slope must be steeper than 0.083; at d_{10}, slope > 0.166; at d_{15}, slope > 0.249; and at d_{20}, slope > 0.332. One can simply use a spreadsheet to plot Eq. 1 passing through any point (d_x, y_x), as shown for three positions in Fig. 1.

In practice, all criteria simply mean that the GSDC should not have a flat portion anywhere and should not end with a flat tail to avoid internal erosion. In a plot, the verification of the three usual criteria is easy. There are three theoretical curves: two straight lines of slopes 0.215 and 0.249 per log cycle, and the curve given by Eq. 1. A spreadsheet enables the user to displace easily the two straight lines and the curve (Eq. 1) by using translation factors. Fig. 1 shows the graphical analyses for the 0-5 mm crushed stone, which was tested for the research presented in this paper.

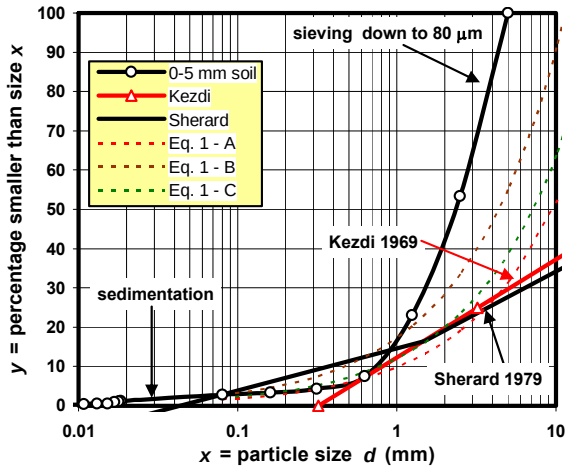

Figure 1. GSDC of the tested 0-5 mm material, with the three criteria of Kezdi (1969), Sherard (1979) and Kenney and Lau (1985) expressed as geometric criteria to assess the potential for internal erosion (Chapuis (1992).

According to Fig. 1 and detailed calculations, the three old criteria agree that the particles smaller than about 0.3 mm are likely to move during seepage.

2.2 Critical criteria for internal erosion

The tested 0-5 mm soil is not uniform and its particles are not rounded: therefore, the criterion for sand boiling does not apply (Chapuis 2009). With the physical characteristics of this soil and its compaction conditions for the tests, the quicksand gradient is close to 1. However, according to Skempton and Brogan (1994), the fine migration for this 0-5 mm soil should start at a gradient between 1/5 and 1/3 of the sand boiling gradient, thus 0.20 and 0.33.

Perzlmaier et al. (2007) proposed a chart based upon $C_U = d_{60}/d_{10}$ and d_{10} to predict the likelihood of internal erosion and critical gradient value. According to their chart (Fig. 2), the fine migration may occur for particles smaller than 0.34 mm and the critical gradient value is 0.31.

Istomina (1957) presented an internal erosion criterion that gives the critical gradient value as a function of C_U. For the tested 0-5 mm soil, his criterion predicts a critical gradient value between 0.3 and 0.4.

All predictive methods agree that solid particles smaller than 0.3–0.34 mm are likely to move within the

soil pore space, and that their movement should start at a gradient value in the 0.2–0.4 range.

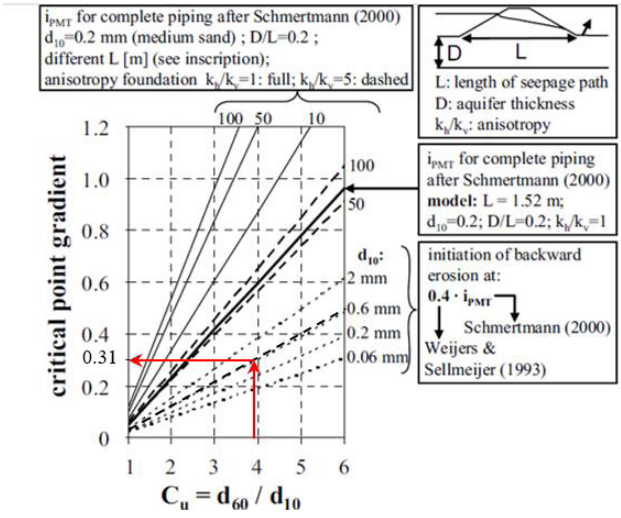

Figure 2. Predictive method of Perzlmaier et al. (2007) for the likelihood of internal erosion.

3 METHODS

The laboratory tests started with a full characterization of the 0-5 mm material. Clear-wall rigid-wall permeameters helped to see and photograph the internal erosion. The tests were performed with either downward or upward seepage, always for fully saturated conditions. The permeability tests were also coupled with non-reactive tracer tests, to determine the effective porosity and compare it to the total porosity of the tested specimen.

3.1 Standard tests for physical properties

The grain size distribution (GSDC) is plotted in Fig. 1. The 0-5 mm material is obtained from crushed limestone. Its specific gravity, G_s, has a value of 2.55. During a Proctor compaction test, the specimen reaches a maximum dry density ρ_d of 1705 kg/m^3 at a water content of 4.2%.

3.2 Tests in rigid-wall permeameters

Permeameters with clear walls were needed to be able to film the migration of particles and the paths of dyed water used as tracer. Thus, rigid-wall permeameters were selected. According to ASTM D2434, the internal diameter of the permeameter must be at least 8 to 10 times the diameter of the largest soil particle, thus at least 50 mm for the 0-5 mm soil. This old rule avoids having poor packing conditions along the wall, and preferential seepage here (Chapuis et al. 2015). The testing program used two permeameters, with respective internal diameters of 8.5 and 10 cm, and height of about 45 cm.

The hydraulic resistance of a permeameter must be lower than that of the tested specimen. The hydraulic head values must be measured within the soil specimen, not only at the entrance and at exit of the permeameter. These rules avoid deriving incorrect values for the gradient and the hydraulic conductivity. For the tests reported here, it was necessary to change the connecting pipes and valves for larger ones because the tested soil had a saturated K value in the range of 10^{-1} cm/s. The hydraulic resistance of the empty permeameters was increased from about 5 x 10^{-2} cm/s up to about 1-2 cm/s.

Figure 3 shows a permeameter, equipped with large connecting pipes and lateral piezometers for that purpose. At the entry, the hydraulic head was kept constant using a 60-L Mariotte bottle filled with deaired water. At the exit, the hydraulic head was kept constant by an overflow.

Figure 3. Experiment with a 60-L Mariotte bottle (not shown) as the constant-head reservoir. An electronic scale measures the water leaving the column. Tracers are injected through a septum in the T connection.

The soil was placed at a moisture content of 4%, in layers about 5-cm-thick. The small water content avoided initial segregation that happens with a dry soil having this GSDC. Compaction was achieved using sliding weight tampers (ASTM D2434) and not heavy masses. The technique of slowly seeping deaired water was retained to increase the degree of saturation (Chapuis 2004a). This technique takes a long time, but is necessary to reach a S_r value in the 98-100% range, which is determined using a mass-and-volume technique (Chapuis et al. 1989).

An example of the increase in the S_r value appears in Fig. 4. The gravimetric water content is low (4 %) during placement. The first inflow of deaired water brings the S_r

value in the 75-80% range, which corresponds to satiation and not full saturation. The slow seepage of deaired water then increases the S_r value to reach a 98-100% range. At a saturation degree S_r, the soil hydraulic conductivity K is $K(S_r)$, whereas ist is Ksat at full saturation.

For comparison, the initial S_r value is in the 80-85% range for rounded grain sand, with a $K(S_r)$ value between K_{sat} / 5 and K_{sat} / 3 (Chapuis et al. 1989), For a silty sand, the initial S_r value may be as low as 65%.

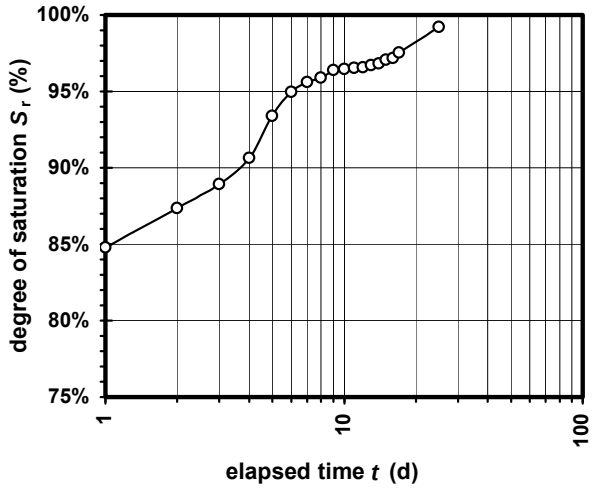

Figure 4. Plot of the degree of saturation, S_r, versus time.

A high S_r value was achieved by long (25 days) seepage of deaired water through the column, at a low gradient to avoid starting internal erosion. Deaired water slowly dissolves tiny gas bubbles, which adhere to solids. These bubbles reduce seepage while adding small uplift forces to small solid particles, and thus interfering with internal erosion when the soil is not saturated,

Permeability tests were done at a low hydraulic gradient to obtain the K value of saturated soil specimens. For comparison, three methods were used to predict the saturated K value: that of Hazen coupled with Taylor (Chapuis 2004b), that of Mbonimpa et al. (2002), and that of Chapuis (2004a). The method of Hazen-Taylor, for the test e value, predicted K = 0.245 cm/s. The method of Mbonimpa et al. (2002) predicted K = 0.19 cm/s. The method of Chapuis (2004b), predicted K = 0.248 cm/s. The method of Kozeny-Carman (Chapuis and Aubertin 2003), which requires a determination of the specific surface, S_S (Chapuis and Légaré 1992), is not reliable when it is used for a soil that is likely to exhibit internal erosion (Chapuis 2012), and it was not retained.

The erosion tests proceeded with either downward seepage or upward seepage. Each test comprised a series of constant mean gradients, which were obtained from hydraulic heads measured within the permeameter, at the bottom and top of specimen, without taking into account the hydraulic head losses at the entry and at the exit of the permeameter.

3.3 Tracer tests in long rigid-wall permeameters

Tracer tests were carried out at different values of the mean gradient, in order to determine the value of effective porosity, n_e, for the specimen, after more or less erosion. Internal erosion develops a few preferential pathways: These were visualized using a non-reactive red dye (food colour). Such a tracer test is economical, but gives an approximate time for the arrival of the color at the end of the specimen. More accurate tracer tests were done with Lithium, which is non-reactive and is measured at the ppb level using atomic adsorption.

The tracers were injected through a septum of the dead end of a T connection (see Fig. 3). The red dye was simply injected with a syringe. The Li-solution was injected by a needle connected to a 1L-Mariotte bottle that maintained the same hydraulic head as the 60-L bottle. The concentration C in Lithium was therefore changed from 0 (60-L bottle) to C_{inj} (constant concentration in the 1L-bottle) by rotating the valves.

In the tracer tests, the total travel time of the tracer include the time to reach the specimen from the injection spot, the time spent within the specimen, and the time between the end of the specimen and the sampling point. This appears schematically in Fig. 5. Simple volume methods yielded the two durations for entrance and exit. These were subtracted from total time, in order to derive the travel time of interest, that within the specimen.

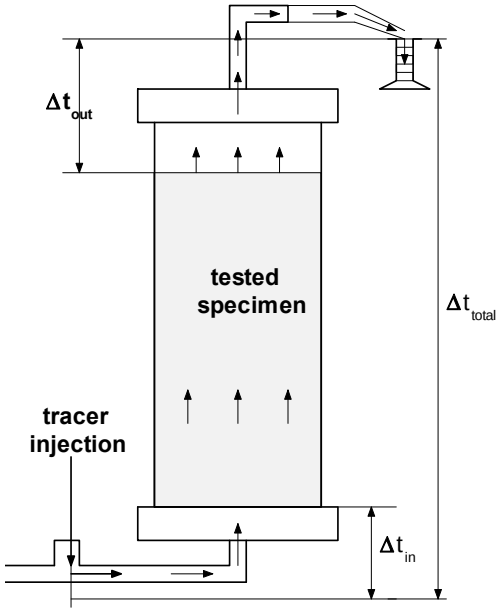

Figure 5: The different times of the tracer tests.

4 RESULTS

The laboratory results are presented first for the erosion tests, and then for the tracer tests.

4.1 Erosion tests

The movement of solid particles was recorded for upward seepage only. For downward seepage, the fine particles were invisible until the end of the test and dismounting of the equipment. In an upward test, the first movement of solids was identified and recorded (video) at a low

gradient of about 0.1. The moving particles formed some dust cloud remaining in suspension (size less than about 0.01 mm) above the specimen, which persisted up to a mean gradient of about 0.3 (Fig. 6).

For mean gradient steps between 0.3 and about 0.7, larger particles could be seen emerging from the top of the specimen. Usually, there were three or four exit zones, clearly identified by the red dye as preferential seepage pathways. For higher mean gradient values, the specimen seemed to internally rearrange, and it had a few locally heaved zones. The soil having angular particles, there was no sand boiling, the particles being able to develop interlocking plus arching against the wall.

The measured *K* value, at the beginning of the test for a low gradient value, was close to that predicted using the three reliable predictive methods (Fig. 7). However, the measured *K* value increased rapidly with the movement of the dust particles, and then, increased more slowly when larger particles, in the 0.01 to 0.3 mm range, moved. During the steps at high gradient values, the *K* value slightly decreased, which is explained by internal rearrangement of the solids within the specimen (Fig. 7).

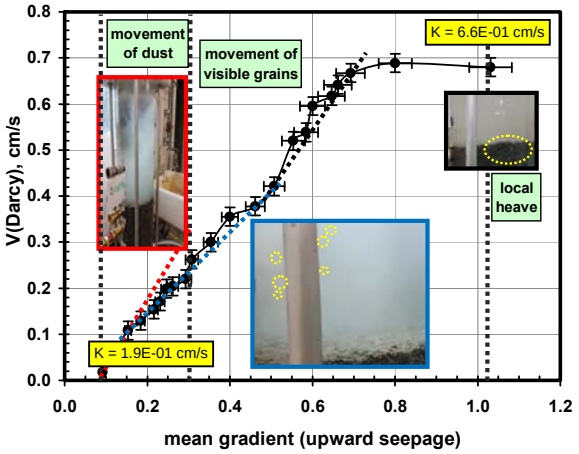

Figure 6. Darcy velocity (cm/s) during an erosion test. Visual correlation with the registered movements of fine particles.

In another erosion test with upward seepage, very low initial gradients were used, and the increase in *K* value appeared to start very rapidly up to a mean gradient of 0.1 (Fig. 8) In this test, tests the *K* value slowly decreased when the internal erosion progressed, between gradients of 0,1 and 0.6. Afterwards, for higher gradients, the *K* value stabilized at over 3 times the predicted *K* value for a homogeneous specimen.

When comparing Figs. 7 and 8, it appears that the internal erosion process was different. It was progressive for the test of Fig. 7, where reorganization of the solid skeleton seemed unimportant during erosion, but active mostly after the end of the erosion. The internal erosion was more sudden for the test of Fig. 8, where the reorganization of the solid skeleton seemed to occur mostly during the erosion process, the preferential pathways being stable after the end of erosion.

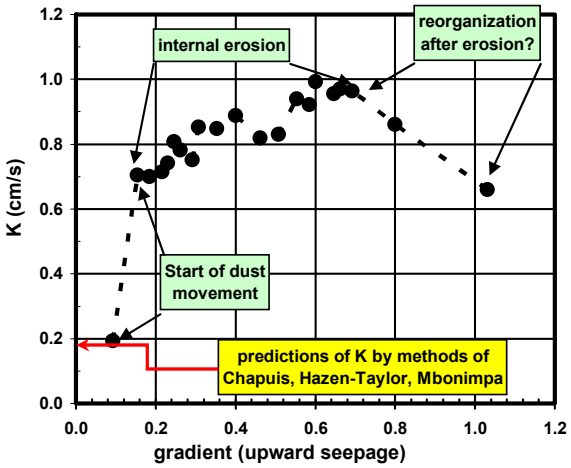

Figure 7. Evolution of the *K* value during an erosion test. The erosion is progressive, and the particle reorganization occurs at the end of the erosion process.

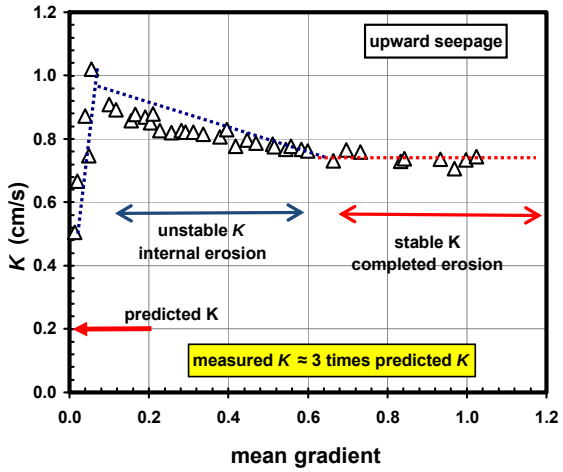

Figure 8. Evolution of the *K* value during an erosion test. The erosion is rapid, and the particle reorganization occurs at the same time as the erosion process.

4.2 Tracer tests

The simple tracer tests with a red dye provided only an estimate of the n_e value. The tracer tests with lithium provided a full breakthrough curve, such as that in Fig. 9.

For the example of Fig. 10, the total porosity *n* of the tested specimen was 34%. Before starting the erosion process, the seepage conditions at a very low gradient verified that the specimen was homogenous (linear hydraulic head losses). The Lithium tracer test gave an effective porosity value of 33%, thus n_e was very close to *n*. This type of result is found systematically with non-plastic homogeneous soil specimens (Ogata and Banks, 1961; Bear 1972; references). Therefore, the tracer test confirmed the observations of hydraulic head distribution with the lateral piezometers; the specimen was homogenous at a very low gradient.

In field conditions, however, especially with stratified aquifers, the n_e value is lower than *n*, which explains the

early arrival of non-reactive tracers (Stephens et al. 1998). This inequality is simply explained by stratification and heterogeneity. Predictive equations were recently developed for the n_e value to be used in a field tracer test (Chapuis 2017, 2018).

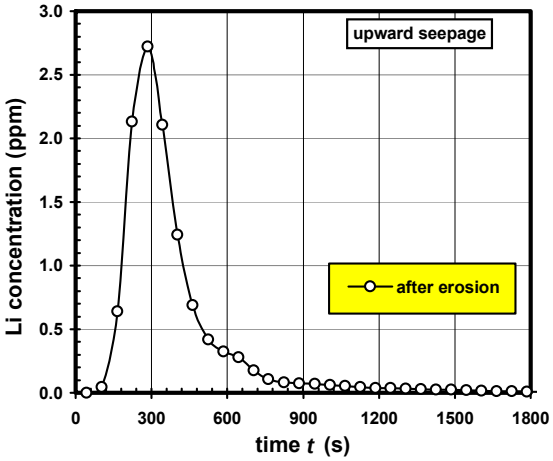

Figure 9. Breakthrough curve of a Lithium tracer test.

During the erosion process, several red dye tracer tests were performed, and indicated that the n_e value was rapidly decreasing before reaching an apparently steady value for gradients higher than 0.23. The n_e value given by the red dye tests was confirmed by a Lithium tracer test, which was performed after the erosion process, at a low constant gradient below 0.1. This Lithium tracer test gave an effective porosity value of 23.5% after erosion, thus confirming that the internal erosion process had created preferential pathways.

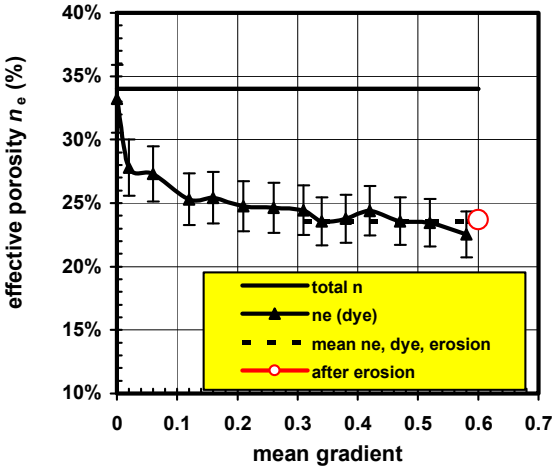

Figure 10. Evolution of the effective porosity, n_e, during the internal erosion process.

5 DISCUSSION AND CONCLUSION

A crushed stone 0-5mm was used for internal erosion tests. The likelihood of internal erosion was assessed theoretically using several criteria. All of them agreed that the particles smaller than about 0.3 mm were likely to move independently within this soil. The criteria also predicted that the internal erosion would start at a gradient close to 0.3.

The real risk was evaluated by tests in clear-wall rigid-wall permeameters, equipped with lateral piezometers. The geometric precautions avoided parasitic wall effects. The compaction precautions made it possible to start with a homogenous specimen. The saturation method made it possible to start with a fully saturated condition. The success of all precautions was verified using several independent methods.

Each internal erosion tests involved several steps at a constant mean gradient, starting with a very small value such as 0.01, and ending with a step at a value close to 1.0. Each test involved a series of gradient steps, the seepage in the vertical permeameter being either downward or upward.

At the beginning of each test, the local gradient values within the long specimen were equal: they indicated that the specimen was homogeneous at the beginning. The measured K value at the beginning of each test was close to 0.2 cm/s. For comparison, three reliable methods that were applicable to predict the K value of the 0-5 mm material. It appeared that the method of Kozeny-Carman predicted unrealistic values, whereas three other methods (combined Hazen-Taylor method described in Chapuis 2004; method of Mbonimpa et al 1992; method of Chapuis 2004) provided close predictions of about 0.2 cm/s. Thud, the correspondence was good between the predicted and measured K values.

Experiments have shown that the evolution of the K value during internal erosion is not a smooth process. This is due to internal reorganization of voids, with local clogging and unclogging.

The displacement of fine particles was observed and filmed in the upward seepage tests. The internal erosion tests created a few visible preferential seepage paths (3-4) for each test. These were visually identified using coloured water as a simple inexpensive tracer test. In addition, non-reactive tracer tests were conducted after a few gradient steps. At least one before the start of erosion, and one after the erosion had been completed.

The internal erosion test of the 0-5 mm soil started with dust (0.001 - 0.01 mm) erosion at a low gradient value, such as 0.1 or less. Erosion of fine particles in the 0.01–0.3 mm range started after dust removal, at a gradient close to 0.3. Erosion ended at a gradient of 0.6-0.7. The range of mobile particles had been correctly predicted for this soil. In addition, the gradient value at which internal erosion would start had been correctly predicted.

The solids within the soil specimen seemed to reorganize during or after the erosion process, which created heave or settlement, depending on the test. This means that the preferential pathways had more or less stable walls, which either resisted or collapsed locally during the internal erosion process.

The first tracer tests, for initial steps at a low gradient and no hydraulic heterogeneity, gave an effective porosity value close to the total porosity, as usually registered with homogenous specimens. During the erosion process, the

effective porosity value decreased markedly. It reached some constant value at the end of the erosion process. This stabilization happened because the created preferential pathways were no longer evolving with time, and had reached some mechanical stability.

Several authors view internal erosion in a non-plastic soil as resulting from some bimodal structure (Skempton and Brogan 1994; Radjai et al. 1998; Indraratna et al. 2011; Moffat and Herrera 2015; To et al. 2015; Vincens et al. 2015). In this view, the large soil particles form an internal structure, which supports most stresses, whereas there are mobile small solids in the voids of this structure. Knowing how to sort the two groups of particles is important to understand and assess the likelihood of internal erosion.

A recent paper (Chapuis and Saucier 2018) has used the modal decomposition method (MDM) to analyze the GSDC of a 0-20 mm soil that was prone to internal erosion. The MDM determined that there were not two but three modes for this material: a fine mode, a medium mode, and a coarse mode. The MDM for sub-specimens after the erosion test has found that the fine mode moved, because it was poorly retained in the load bearing structure formed by the medium and coarse modes. The erosion process was easily quantified by the MDM, which found the same three modes in all parts of the tested specimen. The fine mode was the only mobile mode during the test. Consequently, this recent paper quantified the idea that a first group of particles forms a bearing structure, and that a second group is made of more or less mobile particles in the pore space of the first bearing group. However, the MDM has shown that the bearing structure for the tested material was itself bimodal, which is a little more complex that previously believed.

For the tested material of this paper, the internal erosion could have been quantified by the modal decomposition method of GSDCs (Chapuis et al. 2014; Chapuis 2016). However, this type of analysis takes too much place to be presented in this article, which has space limitations. It will be presented in a next paper.

Acknowledgments

Parts of the investigations on internal erosion processes were subsidized by a NSERC discovery grant.

REFERENCES

ASTM D2434 (2018) Permeability of granular soils (constant head). *Annual Book of ASTM Standards*, West Conshohocken, PA.

Bear, J., 1972, Dynamics of Fluids in Porous Media, *American Elsevier*, New York.

Chang DS, Zhang LM (2013a) Critical hydraulic gradients of internal erosion and suffusion of granular soils. *J Geotech Geoenviron Engng*, **139**(9): 1454–146.7

Chang DS, Zhang LM (2013b) Extended internal stability criteria for soils under seepage. *Soils and Foundations* **53**(4): 569–583.

Chapuis RP (2018a) Tracer tests in stratified alluvial aquifers: predictions of effective porosity and longitudinal dispersivity versus field values. *Geotech Testing J*., in print.

Chapuis, R. P., 2017, "A Simple Reason Explains Why it is so Difficult to *Assess Groundwater Ages and Contamination Ages," Science of the Total Environment*, **593**: 109–115.

Chapuis RP (2016) *Extracting information from grain size distribution curves*. Geotics Editions, Montreal.

Chapuis RP (2012) Predicting the saturated hydraulic conductivity of soils: a review. *Bull Eng Geology Environ*, **71**(3): 401–434.

Chapuis RP (2009) Relating hydraulic gradient, quicksand, bottom heave, and internal erosion of fine particles. *Geotechnical News*, **27**(4): 36–38.

Chapuis RP (2004a) Permeability tests in rigid-wall permeameters: Determining the degree of saturation, its evolution and influence on test results. *Geotech Testing J*, **27**(3): 304–313.

Chapuis RP (2004b) Predicting the saturated hydraulic conductivity of sand and gravel using effective diameter and void ratio. *Can Geotech J*, **41**(5): 787–795.

Chapuis RP (1992) Similarity of internal stability criteria for granular soils. *Can Geotech J*, **29**: 711–713.

Chapuis RP, Aubertin M (2003) On the use of the Kozeny–Carman's equation to predict the hydraulic conductivity of a soil. *Can Geotech J*, **40**(3): 616–628.

Chapuis RP, Légaré PP (1992) A simple method for determining the surface-are of fine aggregates and fillers in bituminous mixtures. In *Effects of Aggregates and Mineral Fillers on Asphalt Mixture Performance*, ASTM STP **1147**: 177–186.

Chapuis RP, Saucier A (2018) Assessing internal erosion with the modal decomposition of grain size distribution curves. *Acta Geotechnica*, submitted.

Chapuis RP, Tournier JP (2006) Simple graphical methods to assess the risk of internal erosion. *Proc ICOLD Barcelona 2006*, Question 86, Balkema, pp. 319–335.

Chapuis RP, Baass K, Davenne L (1989) Granular soils in rigid-wall permeameters: method for determining the degree of saturation. *Can Geotech J*, **26**(1): 71–79.

Chapuis RP, Contant A, Baass K (1996) Migration of fines of 0-20 mm crushed base during placement, compaction, and seepage under laboratory conditions. *Can Geotech J*, **33**: 168–176.

Chapuis RP, Dallaire V, Saucier A (2014) Getting information from modal decomposition of grain size distribution curves. *Geotech Testing J*, **37**(2): 282–295.

Foster MA, Fell R, Spannagle M (2000) The statistics of embankment dam failures and accidents. *Can Geotech J*, **37**: 1000–1024.

Indraratna B, Nguyen VT, Rujikiatkamjorn C (2011) Assessing the potential of internal erosion and suffusion of granular soils. *J Geotech Geoenviron* **137**(5): 550–554.

Istomina V (1957) Filtration stability of soils. *Gostroizdat*, Moscow.

Kenney TC, Lau D (1985) Internal stability of granular filters. *Can Geotech J*, **22**: 215–225.

Kenney TC, Lau D (1986) Reply: Internal stability of granular filters. *Can Geotech J*, **23**(3): 420–423.

Kezdi A (1969) *Increase of protective capacity of flood control dikes* (in Hungarian). Dept of Geotechnique, Tech. University, Budapest, Report No.1.

Li M, Fannin RJ (2008) Comparison of two criteria for internal stability of granular soil. *Can Geotech J*, **45**: 1303–1309.

Li M, Fannin RJ (2012) A theoretical envelope for internal instability of cohesionless soil. *Géotechnique*, **62**(1): 77–80.

Lubochkov EA (1965) Graphical and analytical methods for the determination of internal stability of filters consisting of non cohesive soil (in Russian). *Izvestia, vniig*, **78**: 255–280.

Lubochkov EA (1969) The calculation of suffossion properties of non-cohesive soils when using the non-suffossion analog (in Russian). *Proc. Int Conf Hyd Research,* Brno, Czechoslovakia, Pub Technical University of Brno, Svazek B-5: 135–148.

Mbonimpa M, Aubertin M, Chapuis RP, Brussière B (2002) Practical pedotransfer functions for estimating the saturated hydraulic conductivity. *Geotech. and Geol. Engn*, **20**: 235–259.

Moffat R, Herrera P (2015) Hydromechanical model for internal erosion and its relationship with the stress transmitted by the finer soil fraction. *Acta Geotechnica*, **10**(5): 643–650.

Ogata, A. and Banks, R.B., 1961, "A Solution to the Differential Equation of Longitudinal Dispersion in Porous Media," US Geological Survey, Professional Paper 411–A, 13 p.

Perzlmaier S, Muckenthaler P, Koelewijn AR (2007) Hydraulic Criteria for Internal Erosion in Cohesionless Soil. *Intermediate Report of the European Working Group of ICOLD*, 30–44.

Radjai F, Wolf DE, Jean M, Moreau J (1998) Bimodal character of stress transmission in granular packings. *Physical Review Letters*, **80**(1): 61–64.

Sherard JL (1979) Sinkholes in dams of coarse, broadly graded soils. *Trans 13th ICOLD*, New Delhi, India. Int Com Large Dams, ICOLD, Paris, Vol. 2: 25–35.

Skempton AW, Brogan J (1994) Experiments on piping in sandy gravels. *Geotechnique*, **44**(3): 449–460.

Stephens, D. B., Hsu, K. C., Prieksat, M. A., Ankeny, M. D., Blandford, N., Roth, T. L., and Kelsey, J. A., 1998, "A Comparison of Estimated and Calculated Effective Porosity," Hydrogeology, **6**(1): 156–165.

To HD, Galindo-Torres SA, Scheuermann A (2015) Primary fabric fraction analysis of granular soils. *Acta Geotechnica*, **10**: 375–387.

Vincens E, Witt KJ, Homberg U (2015) Approaches to determine the constriction size distribution for understanding filtration phenomena in granular materials. *Acta Geotechnica*, **10**: 291–303.

Wan CF, Fell R (2008) Assessing the potential of internal instability and suffusion in embankment dams and their foundations. *J Geotech Geoenviron*, **134**(3): 401–407.